Distribution Agreement

In presenting this thesis as a partial fulfillment of the requirements for a degree from Emory University, I hereby grant to Emory University and its agents the non-exclusive license to archive, make accessible, and display my thesis in whole or in part in all forms of media, now or hereafter now, including display on the World Wide Web. I understand that I may select some access restrictions as part of the online submission of this thesis. I retain all ownership rights to the copyright of the thesis. I also retain the right to use in future works (such as articles or books) all or part of this thesis.

Daniela Farchi Behar October 30, 2020

In vivo Characterization of the Critical Interaction between the RNA Exosome and the Essential RNA Helicase Mtr4

by

Daniela Farchi Behar

Anita H. Corbett, Ph.D.

Advisor

Biology Department

Anita H. Corbett, Ph.D.

Advisor

Arri Eisen, Ph.D.

Committee Member

Joseph Moon, Ph. D.

Committee Member

2020

In vivo Characterization of the Critical Interaction between the RNA Exosome and the Essential RNA Helicase Mtr4

By

Daniela Farchi Behar

Anita H. Corbett, Ph.D.

Advisors

An abstract of

a thesis submitted to the Faculty of Emory College of Arts and Sciences

of Emory University in partial fulfillment

of the requirements of the degree of

Bachelor of Science with Honors

Biology Department

2020

Abstract

In vivo Characterization of the Critical Interaction between the RNA Exosome and the Essential RNA Helicase Mtr4

By Daniela Farchi

The RNA exosome is a conserved, exo/endoribonuclease complex that processes/degrades numerous coding and non-coding RNAs. The 10-subunit core RNA exosome is composed of three S1/KH cap subunits (EXOSC2/3/1), a lower ring of six PH-like subunits (EXOSC4/7/8/9/5/6), and a base 3'-5' riboexo/endonuclease subunit, DIS3. RNA processing mutations are the second most common class of mutations linked to multiple myeloma, and mutations in the riboexo/endonuclease gene, *DIS3*, have been repeatedly identified in patients with this disease. Recently, a rare multiple myeloma patient missense mutation was identified in the cap subunit gene *EXOSC2*. This missense mutation results in a single amino acid substitution, M40T, in a highly conserved domain of EXOSC2. Structural studies suggest this M40 residue makes direct contact with the essential RNA helicase, hMtr4, and may stabilize an interaction *in vivo*. We hypothesize that the EXOSC2 substitution M40T destabilizes the interface between the complex and the hMtr4 helicase, thus affecting downstream targeting/processing of the RNA exosome. To test this hypothesis, we generated *Saccharomyces cerevisiae* that express the corresponding EXOSC2 M40T variant, Rrp4 M68T. Cells expressing Rrp4 M68T show no detectable growth defect, suggesting that the essential Mtr4-RNA exosome interaction is functional with the multiple myeloma modeled substitution. However, when we genetically delete other cofactors that are stabilizing partners for Mtr4, *S. cerevisiae* expressing Rrp4 M68T, cells show a severe

growth defect. These data suggest that the introduction of the multiple myeloma mutation impairs the function of the essential RNA exosome, potentially by decreasing the stability of the binding interface between EXOSC2 and hMtr4. To further assess the functional consequences in *S. cerevisiae* Rrp4 M68T cells, we performed RT-qPCR to analyze known RNA exosome target transcripts. By investigating the M40T substitution in *S. cerevisiae*, we provide insight into the functional relevance the M40T substitution could have in disease progression and characterize a key cofactor interface with the RNA exosome *in vivo*.

In vivo Characterization of the Critical Interaction between the RNA Exosome and the Essential RNA Helicase Mtr4

By

Daniela Farchi

Anita H. Corbett, Ph.D.

Advisors

A thesis submitted to the Faculty of Emory College of Arts and Sciences

of Emory University in partial fulfillment

of the requirements of the degree of

Bachelor of Science with Honors

Biology Department

2020

Acknowledgements

I would like to express my deep gratitude to various mentors in the Corbett lab and at Emory who provided me with rich guidance, led my formation, and offered me support in completing my honors thesis. I would like to thank my committee members Dr. Eisen and Dean Moon for your compassion and for your pivotal advice that not only led me to the Corbett lab but without which I would not have been able to complete this work. I am grateful to Milo, Sarah, Agniva, Laramie and Julia for being available to offer valuable insights and for always making time to help me learn. I also want to thank Dr. Lawrence Boise for sharing the patient mutation that became the foundation of this project. Additionally, I extend my appreciation to Sarah Strassler for taking the time to train me in using PyMOL and for sharing her wealth of knowledge that was essential to my understanding of the biochemical principles behind the models.

I am particularly grateful to Maria for always being eager to answer my questions, for sharing her contagious passion for science with me with empathy and kindness, and for encouraging me to constantly grow with her honest feedback (and for never making me feel bad about my terrible mental math skills). Finally, I would like to thank Dr. Corbett for allowing me to join her lab and for her indiscriminate advocacy for me to pursue my goals both in the lab and outside. From both of you I have learned what type of mentorship and passion I aspire to provide to others in the future, and I am excited to be able to someday celebrate a mentee’s progress as warmly as you have celebrated mine.

TABLE OF CONTENTS

FIGURES

INTRODUCTION

The central dogma of molecular biology states that the transfer of genetic information flows from DNA to RNA to protein (Crick, 1970). However, cells in the same organism with an identical genome are able to carry out specialized functions. Through regulation of gene expression, and processing and degradation of RNA, cells maintain functional flexibility despite a relatively condensed genetic code. Furthermore, proper cell function relies on the ability of cells to process and degrade RNA that is no longer useful or that becomes damaged (Cooper et al., 2009). The RNA exosome complex is essential for both RNA processing and decay.

The RNA exosome is a highly conserved riboexo/endonuclease complex that has a pivotal role in 3’ to 5’ processing and degradation of a vast number of RNAs in both the nucleus and cytoplasm (Zinder and Lima, 2017). First identified in budding yeast for its essential role in maturation of ribosomal RNA (Mitchell et al., 1997), the RNA exosome regulates nearly all RNA species (Schneider and Tollervey, 2013) and plays roles in maintaining genome integrity, translation, and cell differentiation through degradative and surveillance pathways (Ogami et al., 2018). The evolutionarily conserved complex is composed of a 9-subunit structural core and a single 3’-5’ riboexo/endonuclease, DIS3. As shown in Figure 1, the 9-subunit structural core is composed of three S1/KH cap subunits (EXOSC2/Rrp4 (Human/*S. cerevisiae*); EXOSC3/Rrp40; EXOSC1/Csl4) and a lower ring of six PH-like subunits (EXOSC4/Rrp41 (Human/*S. cerevisiae*);EXOSC5/Rrp46; EXOSC6/Mtr3; EXOSC7/Rrp42; EXOSC8/Rrp43; EXOSC9/Rrp45) that form a barrel-like structure through which RNA is threaded to DIS3 at the base of the complex.

RNA exosome specificity for RNA target transcripts is conferred through interactions with cofactor proteins. Interacting cofactors aid the RNA exosome in target recognition, unwinding, degradation, and catalysis (Liu et al., 2006). In the nucleus, the RNA exosome complex associates with a distributive 3'-5' exonuclease, Rrp6, and a stabilizing cofactor, Rrp47, which aid in the processing of complex RNA targets (Januszyk and Lima, 2013; Makino et al., 2013). Structural studies show this interaction is facilitated by another cofactor, Mpp6, which provides a platform for direct interaction with the RNA exosome cap (Milligan et al., 2008; Schilders et al., 2007).

The RNA exosome also interacts with RNA helicases, which are thought to assist in RNA substrate unwinding in the nucleus and cytoplasm. A direct interaction with the nuclear helicase Mtr4 is crucial for directing the RNA exosome to its many target transcripts (Weick et al., 2018). Structural studies show that Rrp47, Rrp6, and Mpp6 form composite surfaces that bind Mtr4 to the exosome complex (Falk et al., 2017; Schuch et al., 2014; Wasmuth and Lima, 2017). Mtr4 is a member of larger complexes that have been implicated in other post-transcriptional regulatory pathways (Puno and Lima, 2018; Stuparevic et al., 2013), emphasizing the importance of this Mtr4-RNA Exosome interaction.

A number of disease mutations have been identified in genes encoding RNA exosome subunits. The most frequent disease-linked RNA exosome mutations are mutations in the exo/endoribonuclease gene *DIS3*. Mutations in *DIS3* are frequently found in patients with multiple myeloma which accounts for 15% of lymphohematopoietic malignancies and for 2% of cancer-related deaths (Alexander et al., 2007). Multiple myeloma is a malignant terminally differentiated B (plasma) cell

neuropathy that originates in the bone marrow. This type of cancer is differentiated from other hematopoietic cancers due to the presence of chromosomal aberrations similar to those observed in epithelial cancers including translocations of chromosomes 13 and 14 (Kuehl and Bergsagel, 2002). Risk factors for developing multiple myeloma include exposure to chemical agents and radiation, genetic predisposition, gender, age, and race (Alexander et al., 2007). Chromosome 13, where the *DIS3* gene is located, has a high incidence of mutations and deletions in multiple myeloma (Boyle et al., 2020). Patients with *DIS3* mutations, especially in minor subclones as compared to major subclones, have been found to have decreased longevity, and multiple myeloma-associated *DIS3* mutations have been found to disrupt proper RNA degradation and processing. (Tomecki et al., 2014) (Weißbach et al., 2015). However, additional mechanistic studies are required to understand how mutations in *DIS3* could contribute to pathogenesis in multiple myeloma.

Disease mutations have not only been identified *DIS3*; recently, they have also been identified in genes encoding structural subunits of the RNA exosome. Recent clinical studies have linked missense mutations in structural *EXOSC* genes to distinct, tissue-specific diseases including pontocerebellar hypoplasia and other neurodevelopmental diseases (Morton et al., 2018). Additionally, RNA exosome structural subunit protein deficiencies have also been identified as a cause of disease, including spinal muscular atrophy and myelination problems (Boczonadi et al., 2014; Müller et al., 2015). This growing collection of diseases linked to missense mutations in non-catalytic structural subunits have now been classified as “RNA exosomopathies”. The sheer number and variety of pathologies of these RNA exosomopathies suggest

that structural destabilization of the RNA exosome results in downstream consequences responsible for the development of disease.

Recently, a rare multiple myeloma patient mutation was identified in the RNA exosome cap subunit gene *EXOSC2.* This mutation is similar to other pathogenic missense exosomopathy mutations as it results in a single amino acid substitution of methionine 40 to threonine (M40T). EXOSC2 M40 falls in a highly conserved portion of the N domain of the RNA exosome cap subunit (Figure 2). Structural studies predict the residue exists on an important interface between the complex and the essential helicase MTR4 (Weick et al., 2018). In addition to this interface with EXOSC2, studies in budding yeast suggest that Mpp6 and Rrp47 provide additional binding support and stabilization for Mtr4 (Schuch et al., 2014). A stable interaction between the RNA exosome and MTR4 was found to play a key role in preventing asymmetric mutagenesis and genome destabilization with patterns such as those observed in multiple myeloma patient samples (Lim et al., 2017). The link between EXOSC2 M40T and multiple myeloma, therefore, is most likely not due to a direct disruption of the catalytic properties of the RNA exosome, as is the case for the multiple myeloma mutations in *DIS3*. This mutation may rather disrupt key interactions that result in downstream consequences for targeting and/or processing/degradation of specific transcripts by the RNA exosome. We hypothesize that the EXOSC2 substitution M40T impairs a key interface between the complex and the hMTR4 helicase (*Saccharomyces cerevisiae* Mtr4) that destabilizes this crucial interaction, thus affecting downstream targeting and processing of target transcripts by the RNA exosome. This investigation will characterize the interface between EXOSC2 and MTR4 both *in silico* and *in vivo*, shedding light on the

molecular and functional consequences that may underlie or contribute to multiple myeloma pathology.

We first assessed this interaction *in silico.* We compared our results to predicted effects resulting from the EXOSC G226D substitution, a pathogenic amino acid substitution linked to an RNA exosomopathy. EXOSC2 G226D is not on the interface with Mtr4 but does have predicted consequences in protein stability (Sterrett et al., 2020). To assess the EXOSC2-MTR4 interaction *in vivo,* we utilized the genetic model system *Saccharomyces cerevisiae*. *S. cerevisiae* serves as an ideal model organism for characterizing the RNA exosome and assessing any downstream consequences *in vivo*. As shown in Figure 2A, EXOSC2 is highly conserved in sequence across budding yeast and humans. Furthermore, the EXOSC2-MTR4 interface is highly conserved in *S. cerevisiae,* as is the corresponding yeast residue Rrp4 M68, which is structurally synonymous to EXOSC2 M40 (Figure 2B and 2C). Thus, we generated cells that express the M40T mutation in the *EXOSC2 S. cerevisiae* orthologous gene, *RRP4*. Cells expressing *rrp4-M68T,* corresponding to *EXOSC2-M40T,* show no detectable growth defect, suggesting that the essential Mtr4-RNA exosome interaction is functional even with the multiple myeloma modeled substitution. However, when we genetically delete genes encoding other RNA exosome cofactors that act as stabilizing partners for the RNA exosome-Mtr4 interface, *rrp4-68T* cells show a severe growth defect that can be rescued by overexpression of Mtr4. To further assess the functional consequences resulting from the Rrp4 M68T amino acid substitution on the Mtr4 interface, we performed qPCR to examine defined RNA exosome target transcripts and detected an increase in target transcript levels in *rrp4-M68T* cells. We compared our genetic and

molecular results to *rrp4-G226D* cells, which model the RNA exosomopathy mutation G226D in *EXOSC2.* The *rrp4-G226D* cells have a marked growth defect and changes in target transcript levels (Sterrett et al., 2020) and therefore serve as a point of comparison between these two pathogenic amino acid substitutions in the cap subunit.

Our data suggest that the introduction of the multiple myeloma mutation could decrease the stability of the binding interface between EXOSC2 and MTR4, potentially impairing the function of the essential RNA exosome. Intriguingly, we found that the *rrp4-M68T* cells have distinct genetic interactions as compared to the *rrp4-G226D* cells, suggesting that each pathogenic amino acid substitutions results in distinct *in vivo* functional consequences. Through studying the M68T substitution in *S. cerevisiae* Rrp4 (M40T in human EXOSC2) as the first *in vivo* and *in silico* study of the interface between the Rrp4 and Mtr4, we strive to learn about key binding interfaces which may inform us about multiple diseases linked to the RNA exosome and gain a deeper insight into the biology of this highly conserved and essential complex.

MATERIALS AND METHODS

Saccharomyces cerevisiae strains, plasmids, and chemicals

The chemicals used in this study were obtained from Sigma-Aldrich (St. Louis, MO), United States Biological (Swampscott, MA), or Fisher Scientific (Pittsburgh, PA), unless stated otherwise. All media were prepared by standard procedures (Adams et al., 1997). The *rrp4Δ* cells (ACY2420) have been previously described (Sterrett et al., 2020). Double mutant strains *rrp4Δ mpp6Δ* and *rrp4Δ rrp47Δ* were generated using homologous recombination. A PCR reaction was performed using a plasmid containing the genomic *NAT* antibiotic cassette (pAC1992) and primers that have 5’ and 3’

overhangs complementary to *MPP6* and *RRP47* using pfuUltra high-fidelity polymerase. Amplicons were check through gel electrophoresis with a 1% agarose gel and gel purified using NEB Gel Purification kit. *S. cerevisiae* ACY2420 were transformed with purified PCR products and plated on YEPD media, incubated overnight at 30°C, and then replica-plated onto selective media the following day.

Site-directed mutagenesis

The *rrp4-G226D*-2xMyc mutant plasmid was previously described (Sterrett et al., 2020). The *rrp4-M68T-2xMyc* mutant plasmid was created using the QuikChange II Site-Directed Mutagenesis Kit (Stratagene) with the AC8700 (5'-ACCCTATCTGGActAGAGGTCACGGTAC-3') and AC8701 (5'-GTACCGTGACCTCTagTCCAGATAGGGT-3') oligonucleotides. Phosphorylation of oligonucleotides at 100μM was accomplished through their incubation with 10μM ATP (adenosine triphosphate), T4 PNK (Polynucleotide Kinase) buffer, T4 PNK polymerase and water at 37°C for 1 hour followed by an incubation at 65°C for 20 minutes. A PCR reaction was performed with a plasmid containing the genomic *RRP4* locus using pfuUltra high-fidelity polymerase. Amplicon size was assessed through gel electrophoresis with a 1% agarose gel. Amplicons of the correct size and *RRP4 CEN6 LEU 2x-MYC* plasmid (pAC3474) were digested with Dpn1 and a ligated using T4 DNA ligase. DHSα *E. coli.* were transformed with10μL of ligated product. The mixture was incubated for 30 minutes on ice and then heat shocked for 50 seconds at 42°C. Cells were washed and incubated at 37°C using LB (liquid broth) media for 1 hour and then plated on ampicillin selective plates and incubated at 37°C. Bacterial colonies that grew

were selected and grown. Plasmids were extracted from bacteria using the QIAprep Spin Miniprep Kit (QIAGEN) and sequenced to confirm mutation was incorporated.

Saccharomyces cerevisiae transformations

All *S. cerevisiae* transformations were conducted following the standard Lithium Acetate (LiOAc) protocol (Burke et al., 2000). Strains were grown in a rotating incubator at 30°C to saturation overnight in liquid YEPD (1% yeast extract, 2% peptone, 2% dextrose, in distilled water). Cultures were diluted to a concentration of OD_{600} = 0.33 in 10 mL YEPD, then incubated at 30°C for 3-8 hours depending on the severity of their growth defect. Cells were washed and resuspended using TE/LiOAc to a concentration of 2 x 10^9 cells/mL. Single-stranded carrier DNA, PEG/TE/LiOAc, and depending on reaction purpose, desired PCR product DNA or Plasmid DNA, were added to cells. The mixture was incubated at 30°C in a shaker for 30 minutes and DMSO was added. Following this incubation, cells were heat shocked at 42°C for 15 minutes, washed, and plated onto selective media.

A plasmid shuffle assay was performed to generate *rrp4-M68T* cells. The LEU2 CEN6 *rrp4-M68T* plasmid was transformed into ACY2420 cells and selected for using 5-fluoroorotic acid (5-FOA) plates. Selected colonies were streaked on leucine minimal media plates and then single colonies were streaked out on leucine minimal media plates for technical replicates.

Saccharomyces cerevisiae spotting and optical density growth assays

The *in vivo* viability of *rrp4* variants and the double mutants was assessed through both spotting assays on solid media and optical density growth assays. Yeast cells were incubated at 30°C overnight in Leu- minimal media. Cultures were diluted

and incubated for three hours in rotation at 30°C. Cells expressing the above plasmids and additionally either MTR4 on a uracil plasmid or an empty uracil plasmid (pAC3) were grown in Leu-, Ura- selective media. The optical density was measured at 600 nm and samples were normalized. For spotting assays six ten-fold serial dilutions of 100-microliter total volume were performed for each sample which were spotted on three separate selective -Leu minimal media plates or on three separate selective -Leu -Ura minimal media plates. The plates were incubated separately at 25°C, 30°C or 37°C and imaged daily for 72 hours.

For optical density growth assays, after incubation, samples were diluted to an initial OD_{600} = 0.05 in Leu- minimal media in a 96 well plate. The samples were then placed in a vibrating spectrophotometer at 37°C that measured optical density every 30 minutes and recorded in a BioTek SynergyMx microplate reader with Gen5 v2.04 software over 48 hours. The experiment was conducted measuring technical triplicates. The means for biological triplicates were graphed with error bars representing standard deviation.

Immunoblotting

To analyze protein expression levels of C-terminally Myc-taggedRrp4 and Rrp4 M68T, *RRP4* and *rrp4-M68T* cells were incubated in 2 mL of Leu- minimal medium at 30°C and grown to saturation overnight. Cultures were diluted in 10 mL to an OD_{600} = 0.4 and further incubated at 37°C for 5 hours. Cultures were centrifuged at 3000 RPM for 3 minutes and cell pellets were transferred to microcentrifuge tubes.

Cell lysate preparation was conducted by resuspending pellets in 0.3 ml RIPA-2 Buffer (50 mM Tris-HCl, pH 8; 150 mM NaCl; 0.5% sodium deoxycholate; 1% NP40;

0.1% SDS) supplemented with protease inhibitors [1 mM PMSF; 3 ng/ml PLAC (pepstatin A, leupeptin, aprotinin, and chymostatin)], followed by addition of 300 µl glass beads. Lysates were placed in a Mini Bead Beater 16 Cell Disrupter (Biospec) for 6 × 1 min at 25°C, and centrifuged at 4°C at 12,000 RPM for 10 min.

Protein lysate concentration was determined by Pierce BCA Protein Assay Kit (Life Technologies). Whole cell lysate protein samples (40 µg) were resolved on Criterion 4–20% gradient denaturing gels (Bio-Rad), transferred to nitrocellulose membranes (Bio-Rad) and Myc-tagged Rrp4 proteins were detected with anti-Myc monoclonal antibody 9B11 (1:2000; Cell Signaling). The 3-phosphoglycerate kinase (Pgk1) protein was detected using anti-Pgk1 monoclonal antibody (1:30,000; Invitrogen) as a loading control.

Immunoblots Quantification

Using ImageJ v1.4 software (National Institutes of Health, MD; http://rsb.info.nih.gov/ij/), the band intensities were measured for Rrp4-Myc, rrp4-M68T-Myc, and Pgk-1. Protein percentages of Rrp4-Myc, rrp4-M68T-Myc relative to Pgk-1, and rrp4-M68T-Myc relative to Rrp4-Myc were calculated using Microsoft Excel for Mac 2011 (Microsoft Corporation).

Total RNA isolation

RRP4 and *rrp4-M68T* cells were incubated in 2 mL of Leu- minimal medium at 30°C and grown to saturation overnight. Cultures were diluted in 10 mL to an OD_{600} = 0.4 and further incubated at 37°C for 5 hours. Cultures were centrifuged at 3000 RPM for 3 minutes and cell pellets were transferred to RNAse-free microcentrifuge tubes, resuspended with 1 mL TRIzol (Invitrogen) and 300 µL of glass beads were added.

Cells were vortexed for 4 minutes at 4°C and 250µL of chloroform were added to each sample, which was then vortexed for 15 seconds and incubated at 25°C for 2 minutes. Samples were centrifuged for 10 minutes at 12,000 RPM and the clear top aqueous layer for each was transferred to a clean RNAse-free microcentrifuge tube. To precipitate RNA, 500 µL of isopropanol were added, samples were vortexed for 10 seconds, and centrifuged for 10 minutes at 12,000 RPM. Pellets were washed with 1 ml of 75% ethanol, centrifuged for 5 minutes at 12,000 RPM, and pellets were air-dried for 15 minutes. RNA was resuspended in 50 µl diethylpyrocarbonate (DEPC, Sigma)-treated water and stored at -20°C.

Quantitative RT-PCR

TLC1 ncRNA*, CUT NEL025, and ITS2 rRNA* steady state RNA levels were analyzed through quantitative RT-PCR. Total RNA isolation was *RRP4* and *rrp4-M68T* cells grown at 37°C*.* Total RNA was treated with DNAse I Amplification Grade and then 1 µg of RNA was reverse transcribed with random hexamers following the manufacturer instructions for Moloney murine leukemia virus reverse transcriptase (Invitrogen). Using 10 ng cDNA for three biological replicates, 0.5 µM QuantiTect SYBR Green Master Mix (QIAGEN), Quantitative PCR was performed on technical triplicates of 10 ng cDNA from three biologically independent samples using 0.5 µM primers for *TLC1* ncRNA*, CUT NEL025, or ITS2 rRNA, and ALG9 control primers* on a StepOnePlus Real-Time PCR machine (Applied Biosystems; T_{anneal}: 55°C; 44 cycles). The ΔΔCt method (Livak and Schmittigen, 2001) was used to calculate fold change normalized to ALG9 for ΔΔCt and to the mean RNA levels in *RRP4* cells for ΔΔCt. Fold changes were calculated relative

to *RRP4* control. Standard error of the mean was calculated and presented as error bars and a two-tailed t-test was conducted to determine significance where *p<0.05.

In silico predictions and analysis

Protein Variation Effect Analyzer (PROVEAN) with scores derived from cluster collected sequence computations and a default score threshold of -2.5 (Choi and Chan, 2015), PolyPhen-2, HumDiv (preferred for assessing rare alleles) and HumVar (preferred for assessing mutations with drastic effects that follow Mendelian genetics) (Adzhubei et al., 2010), SNAP2 with a score of 100 representing the strongest effect prediction (Hecht et al., 2015), and Phyre^2 Missense3D (Kelley et al., 2015) were used to generate predictions for structural effects of the Exosc2 M40T, Exosc2 G198D, Rrp4 M68T, and Rrp4 G226D amino acid substitutions. mCSM-PPI2, where the predicted affinity change of the affected protein in kcal/mol was determined by mCSM-PPI2 through the difference in $\Delta\Delta$G of the wild type to the mutant, where increased difference is represented with larger negative numbers (Rodrigues et al., 2019), and PyMOL (LCC, 2015) were used to predict residue neighboring interactions and to develop visual models for the RNA exosome complex (PDB: 6D6R, 4WFD, 5VZJ).

RESULTS

In silico analysis of EXOSC2-M40T and Rrp4-M68T pathogenic amino acid substitutions

To assess the molecular consequences of the pathogenic amino acid substitution M68T, we performed *in silico* analyses of both the human EXOSC2-M40T and our modeled *S. cerevisiae* Rrp4-M68T variant. EXOSC2-G198D/Rrp4-G226D is a previously investigated pathogenic amino acid substitution found in a region of the

exosome cap subunit we used in predictive assays to compare our multiple myeloma-linked substitution to a known deleterious EXOSC2/Rrp4 mutation (Morton et al., 2018; Sterrett et al., 2020).

The software Phyre^2 predicted the multiple myeloma amino acid substitution to have a neutral effect in both EXOSC2 and Rrp4. However, the software programs PROVEAN and SNAP2 predicted the multiple myeloma substitution to be deleterious or have a negative effect on protein stability in both the human and budding yeast model. The Poly-Phen-2 predicted a 54-68% probability of damaging effects as cause of the EXOSC2 M40T mutation, and a 96-99% probability of damaging effects as cause of the Rrp4 M68T mutation. As compared to the scores for EXOSC2-M40T/Rrp4-M68T, the scores for *EXOSC2-G198D*/*Rrp4-G226D* predict strong deleterious and damaging phenotypes. These results are summarized in Figure 3.

The biochemical character changes were assessed for the M40T substitution in EXOSC2 and the corresponding M68T substitution in Rrp4. Using mCSM-PPI2, a decreased affinity for interactions with surrounding residues is predicted for EXOSC2-M40T and the yeast model variant Rrp4-M68T. These results are similar for EXOSC2-G198D and Rrp4-G226D*.* Changes in hydrophobicity, charge, and torsion were determined by Missense3D. EXOSC2-M40T and the yeast model variant Rrp4-M68T undergo a hydrophobic to neutral change; however, there is no change in the residue's net charge. As described previously (Sterrett et al., 2020), EXOSC2-G198D and Rrp4-G226D substitutions change a neutral amino acid to a hydrophilic and charged residue. Torsion is favored for all pathogenic amino acid substitutions and the corresponding

yeast modeled variants, meaning that the phi/psi angles predicted fall within allowed regions for the wild type protein structure (Figure 3).

Specific residue interaction distances were analyzed to determine potential changes in interface stability between EXOSC2/Rrp4 and the helicase Mtr4. EXOSC2 M40 and EXOSC2 T40 present different residue interaction distances to surrounding amino acids. EXOSC2 M40 is 2.8 Å from MTR4 N98, 3.4 Å from MTR4 I1011, 3.4 Å from EXOSC2 L66, and 3.7 Å from MTR4 N1016. EXOSC2 T40 is 3.0 Å from MTR4 N98, 4.5 Å from MTR4 I1011, 3.4 Å from EXOSC2 L66, and 4.7 Å from MTR4 N1016. MTR4 N1016 and I1011 do not appear at a distance that would allow for significant interactions to occur with Rrp4 T68 (Figure 3).

Protein levels and viability are not severely affected in *rrp4-M68T* cells

In order to expand upon these *in silico* predictions and investigate the consequences of this multiple myeloma mutation *in vivo*, we used *S. cerevisiae* as a model organism. We generated the mutant model *rrp4-M68T* cells that express the multiple myeloma mutation in the *EXOSC2* orthologous gene, *RRP4.* We compared the growth of these *rrp4-M68T* cells to the growth of *rrp4-G226D* cells as a comparison to a known pathogenic mutation that has severe consequences for RNA exosome function (Sterrett et al., 2020). Serial dilution and spotting growth assays on solid medium (n=8) of *RRP4, rrp4-M68T*, and *rrp4-G226D* cells were conducted at 25°C, 30°C, 37°C (Figure 4A). In addition, cell growth was assessed through a liquid growth assay at 37°C (Figure 4B). There was no growth defect detected for *rrp4-M68T* cells at any temperature in either the solid media or liquid media growth assays as compared to wildtype *RRP4* cells.

We next tested whether the protein levels of Rrp4 are affected by the multiple myeloma amino acid substitution. Am immunoblot was performed with protein lysate collected from *RRP4* and *rrp4-M68T* cells grown at 30°C or 37°C. No significant difference in steady state protein levels was observed at either temperature for Rrp4 and Rrp4-M68T, with Rrp4-M68T levels being 97+/-8% of Rrp4 at 30°C and 118+/-20% of Rrp4 at 37°C. These observations follow the *in silico* assays of Rrp4-M68T, which predict no severe structural or biochemical effects as a cause of the amino acid substitution. Therefore these data show the protein expression levels and viability are not severely affected in *rrp4-M68T* cells, though molecular consequences for the function of the RNA exosome could still occur *in vivo* due to destabilization of key interactions.

rrp4-M68T cells have changes in RNA exosome target _TLC1 ncRNA_ steady state levels

To assess molecular consequences for RNA exosome function within *rrp4-M68T* cells, we measured the steady-state level of known RNA exosome target RNAs, the *CUT NEL025, TLC1 ncRNA, and ITS2 rRNA.* We conducted RT-qPCR analysis using total RNA extracted from *RRP4* and *rrp4-M68T* cells grown at 37°C (n=3) (Figure 5). We observed an increase in steady state levels of the known RNA exosome target *TLC1 precursor ncRNA* transcript in *rrp4-M68T* cells. An increase in steady state levels of *TLC1 ncRNA* was previously reported for *rrp4-G226D* (Sterrett et al., 2020). The expression levels of *CUT NEL025* and *ITS2 rRNA* were not significantly affected relative to those in *RRP4* cells in either *rrp4-M68T* or *rrp4-G226D.* These data suggest that though viability of *rrp4-G226D* and *rrp4-M68T* cells differ, both pathogenic amino acid

substitutions result in molecular consequences in the processing/degradation of specific RNA exosome targets.

Deletion of *MPP6* and *RRP47* reveals severe growth defect in *rrp4-M68T* cells

Molecular analyses suggest *rrp4-M68T* cells have impaired function in the RNA exosome, which we predict is due to destabilization of the essential interaction with Mtr4. In the human system, the MTR4-RNA exosome interaction is stabilized through additional interactions with cofactors RRP47 and MPP6 (Figure 6) (Schuch et al., 2014; Stuparevic et al., 2013). In order to investigate the destabilization that could result from the M40T substitution, we utilized the power of yeast genetics and deleted the non-essential yeast cofactor genes *MPP6* and *RRP47* in the *rrp4-M68T* cells (Figure 7). As reported previously, there are no growth defects in *RRP4* cells upon a loss of *MPP6* (Sterrett et al., 2020; Wasmuth et al., 2017). Loss of *MPP6* in *rrp4-M68T* cells, however, causes significant growth defects at all temperatures that were not evident when *MPP6* was present. Loss of *RRP47* in *rrp4-M68T* cells also results in growth defects, though indistinguishable from those observed in *RRP4 rrp47Δ* cells. This growth defect with loss of *RRP47* in both cells is most likely due to the destabilization of the interaction between the catalytic exonuclease Rrp6 and the RNA exosome complex. We compared these results to the growth defects observed in *rrp4-G226D mpp6Δ* and *rrp4-G226D rrp47Δ* double mutants as previously described (Sterrett et al., 2020). Loss of *MPP6* in *rrp4-G226D* cells exacerbates the already severe growth defect that results from this pathogenic amino acid substitution, suggesting that both *rrp4-M68T* and *rrp4-G226D* models exhibit specific genetic interactions with *MPP6*. We rescued the growth defects seen with loss of *MPP6* and *RRP47* by re-introducing these cofactors with

overexpression plasmids (n=5) (Figure 8). These data indicate that the negative genetic interaction observed in both *rrp4* mutant models with *MPP6* can be overcome by overexpression of the cofactor Mpp6. These results demonstrate that the M40T amino acid substitution can alter this critical protein interface.

Overexpression of Mtr4 rescues growth defect of *rrp4-M68T ⊿mpp6* cells

To assess the Mtr4-RNA interface in *rrp4-M68T* cells, we took advantage of the growth defect detected in the double mutant strains and overexpressed Mtr4 in the *rrp4-M68T mpp6Δ* and *rrp4-M68T rrp47Δ* cells (n=3) (Figure 9). We utilized the *rrp4-G226D mpp6Δ* and *rrp4-G226D rrp47Δ* cells as a control for a pathogenic amino acid substitution in the cap subunit that is not predicted to affect the Mtr4 interface. Overexpression of Mtr4 in *rrp4-M68T mpp6Δ* cells rescues growth at 25°C and 37°C. We do not observe this rescue in growth with overexpression of Mtr4 in *rrp4-G226D mpp6Δ* cells. This rescue is specific to the *rrp4-M68T mpp6Δ* cells as overexpression of Mtr4 in *rrp4-M68T rrp47Δ* or *rrp4-G226D rrp47Δ* cells does not improve growth at any temperature. This finding suggests that increased Mtr4 cannot overcome the destabilization of the interaction between the RNA exosome and Rrp6. Therefore, these data suggest that the growth defect seen with a loss of *MPP6* in the *rrp4-M68T* cells can be overcome by introducing more Mtr4 helicase into the system.

DISCUSSION

The EXOSC2-M40T missense mutation identified in a multiple myeloma patient potentially interrupts an important interface between the RNA exosome and the essential MTR4 helicase. In this study, we characterized the interface between EXOSC2 and MTR4 both *in silico* and *in vivo* by exploring how this crucial interaction is

impacted by the EXOSC2 substitution M40T through the orthologous missense mutation, *rrp4-M68T* modeled in *S. cerevisiae*.

Predictive *in silico* analysis does not suggest that the multiple myeloma mutation on its own would lead to effects as severe as those predicted for *rrp4-G226D*, which is a known pathogenic mutation (Sterrett et al., 2020), however this analysis does suggest potential deleterious phenotypes. When modeled in yeast, *rrp4-M68T* cells show no detectable growth defect or changes in protein levels, suggesting that the essential MTR4-RNA exosome interaction is functional even with the multiple myeloma modeled substitution in an otherwise wildtype background. When we genetically delete cofactors that are stabilizing partners for Mtr4, Rrp47 and Mpp6, *rrp4-M68T* cells show a severe growth defect that is rescued when the cofactors are expressed on plasmids. Furthermore, overexpression of Mtr4 rescues the growth defects observed previously for *⊿mpp6 rrp4-M68T* at 25ºC and 37ºC but not for *⊿mpp6 rrp4-G226D cells.* Thus, our data suggest that the introduction of the multiple myeloma-related mutation, *rrp4-M68T*, in *S. cerevisiae* impairs the function of the essential RNA exosome, potentially by decreasing the stability of the binding interface between EXOSC2/Rrp4 and MTR4/Mtr4.

Predictive *in silico* analysis did not yield conclusive results that the *rrp4-M68T* or the *EXOSC2-M40T* mutations would induce severe structural effects. Although some software predicted potential deleteriousness, the biochemical changes provoked by the methionine to threonine substitution did not suggest a severe structural hindrance that would prevent the subunit to associate into the complex (Figure 2). These predictions are supported by the normal growth and steady protein levels observed for Rrp4 in *rrp4-M68T* cells (Figure 4). The presented structural models and analyses are limited, as

they do not take into account the structural rearrangement induced by the Met to Thr amino acid substitution. The residue is nested near two beta sheets and due to the favorability of threonine in coordinating interactions with neighboring beta strands, (Smith and Regan, 1997), the architecture of the surrounding protein could undergo a conformational alteration. Possibly, this alteration could interrupt the interaction between EXOSC2 and MTR4 beyond the predicted loss of the I1011 bond which is due to threonine having lower potential for hydrophobic interactions than methionine (Li et al.).

Despite the structural predictions, the increase in steady-state levels of the known RNA exosome target *TLC1* non-coding telomerase RNA in *rrp4-M68T* cells suggests that the mutation does have molecular consequences. Mature *TLC1* serves as a template for telomere reverse transcription and recruits proteins to ensure telomere integrity (Matsuguchi and Blackburn, 2016). Mtr4 is involved adequate processing of *TLC1* and, consequently, telomere preservation in yeast (Wu, 2015). Steady state levels for *TLC1* ncRNA increase more in *rrp4-M68T* cells than detected in *rrp4-G226D* cells, providing evidence that the M->T substitution does alter the function of the RNA exosome.

We utilized yeast genetics to further assess whether the amino acid substitution could alter the interaction with the critical RNA helicase Mtr4 in the *rrp4-M68T* cells. By generating deletions of the non-essential cofactor genes *MPP6* and *RRP47,* we removed the stabilization provided for Mtr4 by the Mpp6 and Rrp47 cofactors, allowing a more nuanced evaluation of the *rrp4-M68T* mutation RNA exosome-helicase interface. Although there was a growth defect observed in *Δrrp47 RRP4* and *Δrrp47 rrp4-M68T* cells, indistinguishable to that which had previously been reported for *Δrrp47 rrp4-*

G226D cells *(Sterrett et al., 2020),* the results obtained do not detract from the evidence supporting the stabilization of Mtr4 by *Rrp4-M68.* As Rrp47 coordinates with Rrp6 to form a surface which recruits and anchors Mtr4 to the RNA exosome (Schuch et al., 2014), it is likely that loss of Rrp47 decreases the interaction with Rrp6 in all cells (Januszyk and Lima, 2013).

The growth defect observed in Δ*mpp6 rrp4-M68T* cells and that was not evident when the cofactor was present or in Δ*mpp6 RRP4* supports our hypothesis of the important role the Rrp4-M68 residue plays in the stabilization of Mtr4 (Weick et al., 2018). Thus, the *Δmpp6 rrp4-M68T* cells lend us an *in vivo* system to investigate the effects of the pathogenic amino acid substitution on the stabilization of the Mtr4 interaction directly.

The strongest evidence supporting our hypothesis comes from the observation that Mtr4 overexpression rescues the growth defect of *Δmpp6 rrp4-M68T* cells differentially from *Δmpp6 rrp4-G226D* cells. We predict that the growth defect in *Δmpp6 rrp4-M68T* is ameliorated as a higher concentration of Mtr4 becomes available to bind to the RNA exosome and thus increases the probability for complexes to form through increasing one of the binding partners. We have not yet quantified Mtr4 protein levels nor tested if overexpression increases protein binding with Rrp4 M68T. However, overexpression of Mtr4 rescues the growth defects observed previously for *Δmpp6 rrp4-M68T* cells and not for *Δmpp6 rrp4-G226D* cells. The differential rescue of the *Δmpp6 rrp4-M68T* and *Δmpp6 rrp4-G226D* cells by overexpression of Mtr4 suggests that these different pathogenic amino acid substitutions result in specific and distinct molecular consequences in RNA exosome cofactor interactions. The lack of a rescue for all *Δrrp47*

cells is again likely due to the interrupted interaction with the catalytic Rrp6 decreasing the nuclear RNA exosome-mediated processing and degradation activity. Future studies are needed to quantify the threshold at which overexpression of Mtr4 could inhibit Rrp6 binding. This would allow for the optimization of the approach taken to investigate how *rrp4-M68T* impacts Mtr4 binding without the influence of Rrp47. These data suggest that the introduction of the multiple myeloma-related mutation, *rrp4-M68T*, in *S. cerevisiae* does impair the function of the essential RNA exosome, potentially by decreasing the stability of the binding interface between Rrp4 and Mtr4.

Despite being within the same subunit protein, the *rrp4-M68T* and *rrp4-G226D* mutations give rise to different growth phenotypes. These residues have different roles in Rrp4 (Cvetkovic et al., 2017). The *rrp4-G226D* mutation models that of a patient mutation (EXOSC2-G198D) which leads to severe developmental impairment in humans, and to temperature dependent growth defects and downstream effects of a variety of transcripts in *S. cerevisiae* (Sterrett et al., 2020). The *EXOSC2-M40T* mutation is a passenger mutation in a single multiple myeloma patient and the effects of the corresponding *rrp4-M68T* mutation in *S. cerevisiae* are more subtle. While the *rrp4-G226D* mutation likely impacts the structural integrity of Rrp4 in a way that impairs the catalytic activities of the complex (Sterrett et al., 2020), the *rrp4-M68T* mutation likely plays a role in coordinating the interactions of the RNA exosome with Mtr4. In considering how the M40T in EXOSC2 could contribute to cancer phenotypes, one possibility is that RNAs that depend on the function of the RNA helicase MTR4 may be most affected. While there is no catalogue of specific target transcripts that depend on the function of MTR4, this RNA helicase is thought to help unwind structured RNAs for

processing or degradation by the RNA exosome. If some of these RNAs encode pro-growth factors, this could contribute to cancer phenotypes. Future studies could assess whether the *rrp4-M68T* cells show altered cell cycle profiles. Such experiments are straightforward in the yeast model and we could continue the comparison to the *rrp4-G226D* cells. Future studies could also employ an unbiased approach such as RNA sequencing to define the RNAs that either increase or decrease in *rrp4-M68T* cells. This would help to identify any candidate cell cycle genes or other growth regulatory factor genes that could be misregulated in these cells, which could then be extended into the patient cells to test whether orthologous transcripts are altered in those cells. Ultimately, the goal is to exploit the budding yeast model system to provide insights into how specific disease mutations in the RNA exosome could alter the function of this complex and potentially contribute to pathogenesis.

This combined *in silico* and *in vivo* approach to analyzing the effects of the *EXOSC2-M40T* mutation identified in a multiple myeloma patient allowed us to better understand an important interface between the RNA exosome and important cofactors such as Mtr4. With this insight, we gained knowledge about the structural impacts of the amino acid substitution and about the potential downstream effects that the passenger mutation could cause in the patient. A similar approach could be undertaken to analyze other potentially pathogenic mutations that lie in important interfaces of the RNA exosome complex and essential cofactors, such as the prevalent disease-driving mutations that occur in the *DIS3* catalytic subunit of the RNA exosome in many multiple myeloma patients (Boyle et al., 2020). To the best of our knowledge, this study represents the first time that multiple myeloma mutations that occur in genes that

encode components of the RNA exosome have been modeled in the budding yeast system. Due to the evolutionary conservation of this complex, there is the potential to analyze many additional mutations in this manner to understand whether these mutations all impact the function on the RNA exosome in a similar manner or whether different RNAs are impacted. Such studies could provide mechanistic insight into the biological pathways that are altered in this very devastating cancer and thus identify new pathways for therapeutic intervention.

CONNECTION TO CULTURE AND SOCIETY

(FOR SCIENCE, CULTURE AND SOCIETY MINOR)

Chemical agents and radiation exposure have been correlated to the development of multiple myeloma and other lymphohematopoietic malignancies (Alexander et al., 2007; Gold et al., 2011). Individuals in populations undertaking agricultural practices associated with exposure to chemical agent pesticides are often vulnerable to disease and these individuals may face a larger challenge in accessing healthcare (Curl et al., 2020). Immigrant workers facing these conditions are often physically and economically exploited, and a collection of factors including legal documentation and discrimination have the potential to contribute to increased negative health outcomes (Moyce and Schenker, 2018). Considering mutations in the *DIS3* catalytic subunit of the RNA exosome have been identified with a high prevalence in multiple myeloma and other lymphohematopoietic malignancies, it is likely that they are common among this population. Among the common *DIS3* mutations identified were two isoforms of the protein distinguished by the deletion of a portion of the endonuclease PIN domain in one of these isoforms (Robinson et al., 2018). A change in

the ratio in which the isoforms exist could be indicative of hematological malignancies (Robinson et al., 2018). Given that the deletion in the PIN domain of DIS3 could impair the catalytic activity of the RNA exosome, the approach taken in this thesis to elucidate interaction changes could be insightful. The predictive software outlined could be used to determine how the deletion, among other mutations in the *DIS3* subunit, that lead to hematological malignancies affect the structural integrity of the RNA exosome. Further, the collected information could serve as a base for assays to explore misprocessing of RNA with potential links to disease and ultimately identify specific biological pathways that could be targeted for future therapeutic interventions.

REFERENCES

Adams, A., Gottschling, D.E., Kaiser, C.A., and Steams, T. (1997). Methods in Yeast Genetics (Cold Spring Harbor, NY: Cold Spring Harbor Laboratory Press).

Adzhubei, I.A., Schmidt, S., Peshkin, L., Ramensky, V.E., Gerasimova, A., Bork, P., Kondrashov, A.S., and Sunyaev, S.R. (2010). A method and server for predicting damaging missense mutations. Nat. Methods *7*, 248–249.

Alexander, D.D., Mink, P.J., Adami, H.-O., Cole, P., Mandel, J.S., Oken, M.M., and Trichopoulos, D. (2007). Multiple myeloma: A review of the epidemiologic literature. Int. J. Cancer *120*, 40–61.

Boczonadi, V., Müller, J.S., Pyle, A., Munkley, J., Dor, T., Quartararo, J., Ferrero, I., Karcagi, V., Giunta, M., Polvikoski, T., et al. (2014). EXOSC8 mutations alter mRNA metabolism and cause hypomyelination with spinal muscular atrophy and cerebellar hypoplasia. Nat. Commun. *5*.

Boyle, E.M., Ashby, C., Tytarenko, R.G., Deshpande, S., Wang, H., Wang, Y., Rosenthal, A., Sawyer, J., Tian, E., Flynt, E., et al. (2020). *BRAF* and *DIS3* Mutations Associate with Adverse Outcome in a Long-term Follow-up of Patients with Multiple Myeloma. Clin. Cancer Res. 1078-0432.CCR-19–1507.

Burke, D., Dawson, D., and Steams, T. (2000). Methods in yeast genetics: a Cold Spring Harbor Laboratory course manual.

Choi, Y., and Chan, A.P. (2015). PROVEAN web server: a tool to predict the functional effect of amino acid substitutions and indels. Bioinformatics *31*, 2745–2747.

Cooper, T.A., Wan, L., and Dreyfuss, G. (2009). RNA and Disease. Cell *136*, 777–793.

Crick, F. (1970). Central Dogma of Molecular Biology. 3.

Curl, C.L., Spivak, M., Phinney, R., and Montrose, L. (2020). Synthetic Pesticides and Health in Vulnerable Populations: Agricultural Workers. Curr. Environ. Health Rep. *7*, 13–29.

Cvetkovic, M.A., Wurm, J.P., Audin, M.J., Schütz, S., and Sprangers, R. (2017). The Rrp4-exosome complex recruits and channels substrate RNA by a unique mechanism. Nat. Chem. Biol. *13*, 522–528.

Falk, S., Bonneau, F., Ebert, J., Kögel, A., and Conti, E. (2017). Mpp6 Incorporation in the Nuclear Exosome Contributes to RNA Channeling through the Mtr4 Helicase. Cell Rep. *20*, 2279–2286.

Gold, L.S., Stewart, P.A., Milliken, K., Purdue, M., Severson, R., Seixas, N., Blair, A., Hartge, P., Davis, S., and De Roos, A.J. (2011). The Relationship between Multiple Myeloma and Occupational Exposure to Six Chlorinated Solvents. Occup. Environ. Med. *68*, 391–399.

Hecht, M., Bromberg, Y., and Rost, B. (2015). Better prediction of functional effects for sequence variants. BMC Genomics *16*, S1.

Januszyk, K., and Lima, C.D. (2013). Structural Components and Architectures of RNA Exosomes (Landes Bioscience).

Kelley, L.A., Mezulis, S., Yates, C.M., Wass, M.N., and Sternberg, M.J. (2015). The Phyre2 web portal for protein modelling, prediction and analysis. Nat. Protoc. *10*, 845–858.

Kuehl, W.M., and Bergsagel, P.L. (2002). Multiple myeloma: evolving genetic events and host interactions. Nat. Rev. Cancer *2*, 175–187.

LCC, S. (2015). The PyMOL Molecular Graphics System.

Li, J., Ma, X., Zhang, H., Hou, C., Shi, L., Guo, S., Zheng, B., Ye, L., Yang, L., and He, X. The role of hydrophobic interactions in folding of β-sheets. 49.

Lim, J., Giri, P.K., Kazadi, D., Laffleur, B., Zhang, W., Grinstein, V., Pefanis, E., Brown, L.M., Ladewig, E., Martin, O., et al. (2017). Nuclear Proximity of Mtr4 with RNA exosome restricts DNA mutational asymmetry. Cell *169*, 523-537.e15.

Liu, Q., Greimann, J.C., and Lima, C.D. (2006). Reconstitution, activities, and structure of the eukaryotic RNA exosome. Cell *127*, 1223–1237.

Livak, K.J., and Schmittigen, T.D. (2001). Analysis of relative gene expression data using real-time quantitative PCR and the 2(-Delta C(T)) Method. Methods *25*, 402–408.

Makino, D.L., Baumgärtner, M., and Conti, E. (2013). Crystal structure of an RNA-bound 11-subunit eukaryotic exosome complex. Nature *495*, 70–75.

Matsuguchi, T., and Blackburn, E. (2016). The yeast telomerase RNA, TLC1, participates in two distinct modes of TLC1-TLC1 association processes in vivo. PeerJ *4*.

Milligan, L., Decourty, L., Saveanu, C., Rappsilber, J., Ceulemans, H., Jacquier, A., and Tollervey, D. (2008). A Yeast Exosome Cofactor, Mpp6, Functions in RNA Surveillance and in the Degradation of Noncoding RNA Transcripts. Mol. Cell. Biol. *28*, 5446–5457.

Mitchell, P., Petfalski, E., Shevchenko, A., Mann, M., and Tollervey, D. (1997). The Exosome: A Conserved Eukaryotic RNA Processing Complex Containing Multiple 3′→5′ Exoribonucleases. Cell *91*, 457–466.

Morton, D.J., Kuiper, E.G., Jones, S.K., Leung, S.W., Corbett, A.H., and Fasken, M.B. (2018). The RNA exosome and RNA exosome-linked disease. RNA *24*, 127–142.

Moyce, S.C., and Schenker, M. (2018). Migrant Workers and Their Occupational Health and Safety. Annu. Rev. Public Health *39*, 351–365.

Müller, J.S., Giunta, M., and Horvath, R. (2015). Exosomal Protein Deficiencies: How Abnormal RNA Metabolism Results in Childhood-Onset Neurological Diseases. J. Neuromuscul. Dis. *2*, S31–S37.

Ogami, K., Chen, Y., and Manley, J.L. (2018). RNA Surveillance by the Nuclear RNA Exosome: Mechanisms and Significance. Non-Coding RNA *4*, 8.

Puno, M.R., and Lima, C.D. (2018). Structural basis for MTR4-ZCCHC8 interactions that stimulate the MTR4 helicase in the nuclear exosome-targeting complex. Proc. Natl. Acad. Sci. U. S. A. *115*, E5506–E5515.

Robinson, S.R., Viegas, S.C., Matos, R.G., Domingues, S., Bedir, M., Stewart, H.J.S., Chevassut, T.J., Oliver, A.W., Arraiano, C.M., and Newbury, S.F. (2018). DIS3 isoforms

vary in their endoribonuclease activity and are differentially expressed within haematological cancers. Biochem. J. *475*, 2091–2105.

Rodrigues, C.H.M., Myung, Y., Pires, D.E.V., and Ascher, D.B. (2019). mCSM-PPI2: predicting the effects of mutations on protein–protein interactions. Nucleic Acids Res. *47*, W338–W344.

Schaeffer, D., Tsanova, B., Barbas, A., Reis, F.P., Dastidar, E.G., Sanchez-Rotunno, M., Arraiano, C.M., and van Hoof, A. (2009). The exosome contains domains with specific endoribonuclease, exoribonuclease and cytoplasmic mRNA decay activities. Nat. Struct. Mol. Biol. *16*, 56–62.

Schilders, G., van Dijk, E., and Pruijn, G.J.M. (2007). C1D and hMtr4p associate with the human exosome subunit PM/Scl-100 and are involved in pre-rRNA processing. Nucleic Acids Res. *35*, 2564–2572.

Schneider, C., and Tollervey, D. (2013). Threading the barrel of the RNA exosome. Trends Biochem. Sci. *38*, 485–493.

Schuch, B., Feigenbutz, M., Makino, D.L., Falk, S., Basquin, C., Mitchell, P., and Conti, E. (2014). The exosome-binding factors Rrp6 and Rrp47 form a composite surface for recruiting the Mtr4 helicase. EMBO J. *33*, 2829–2846.

Sikorski, R.S., and Hieter, P. (1989). A system of shuttle vectors and yeast host strains designed for efficient manipulation of DNA in Saccharomyces cerevisiae. Genetics *122*, 19–27.

Smith, C.K., and Regan, L. (1997). Construction and Design of β-Sheets. Acc. Chem. Res. *30*, 153–161.

Sterrett, M.C., Enyenihi, L., Leung, S.W., Farchi, D., Kremsky, I., van Hoof, A., Corbett, A.H., and Fasken, M.B. (2020). A BUDDING YEAST MODEL OF EXOSC2 DISEASE MUTATIONS REVEAL DISTINCT DEFECTS IN RNA EXOSOME FUNCTION IN VIVO.

Stuparevic, I., Mosrin-Huaman, C., Hervouet-Coste, N., Remenaric, M., and Rahmouni, A.R. (2013). Cotranscriptional Recruitment of RNA Exosome Cofactors Rrp47p and Mpp6p and Two Distinct Trf-Air-Mtr4 Polyadenylation (TRAMP) Complexes Assists the Exonuclease Rrp6p in the Targeting and Degradation of an Aberrant Messenger Ribonucleoprotein Particle (mRNP) in Yeast. J. Biol. Chem. *288*, 31816–31829.

Tomecki, R., Drazkowska, K., Kucinski, I., Stodus, K., Szczesny, R.J., Gruchota, J., Owczarek, E.P., Kalisiak, K., and Dziembowski, A. (2014). Multiple myeloma-associated hDIS3 mutations cause perturbations in cellular RNA metabolism and suggest hDIS3 PIN domain as a potential drug target. Nucleic Acids Res. *42*, 1270–1290.

Wasmuth, E.V., and Lima, C.D. (2017). The Rrp6 C-terminal domain binds RNA and activates the nuclear RNA exosome. Nucleic Acids Res. *45*, 846–860.

Wasmuth, E.V., Zinder, J.C., Zattas, D., Das, M., and Lima, C.D. (2017). Structure and reconstitution of yeast Mpp6-nuclear exosome complexes reveals that Mpp6 stimulates RNA decay and recruits the Mtr4 helicase. ELife *6*, e29062.

Weick, E.-M., Puno, M.R., Januszyk, K., Zinder, J.C., DiMattia, M.A., and Lima, C.D. (2018). Helicase-dependent RNA decay illuminated by a cryo-EM structure of a human nuclear RNA exosome-MTR4 complex. Cell *173*, 1663-1677.e21.

Weißbach, S., Langer, C., Puppe, B., Nedeva, T., Bach, E., Kull, M., Bargou, R., Einsele, H., Rosenwald, A., Knop, S., et al. (2015). The molecular spectrum and clinical impact of DIS3 mutations in multiple myeloma. Br. J. Haematol. *169*, 57–70.

Wu, H. (2015). Analyses of the Life Cycle of TLC1 and the Nuclear RNA Quality Control System in Saccharomyces cerevisiae (Georg-August University School of Science (GAUSS)).

Zinder, J.C., and Lima, C.D. (2017). Targeting RNA for processing or destruction by the eukaryotic RNA exosome and its cofactors. Genes Dev. *31*, 88–100.

FIGURES

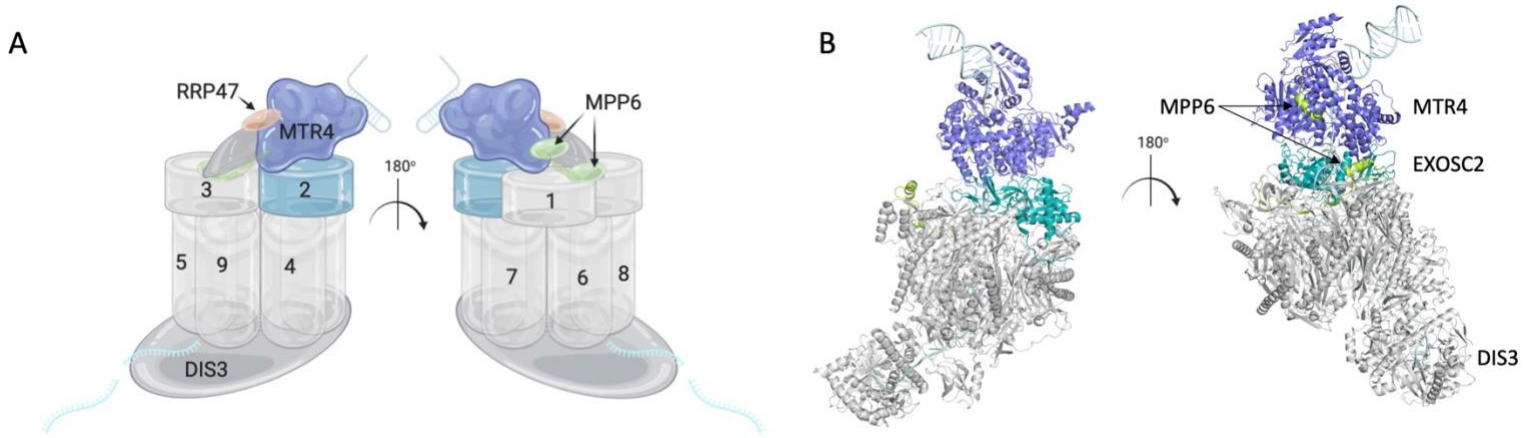

Figure 1. RNA exosome model and structure. A) A cartoon model of the RNA exosome complex is shown including select cofactors of interest, MTR4, MPP6, and RRP47. The RNA exosome is a multi-subunit complex composed of a 9-subunit structural core (EXOSC2/3/1/4/7/8/9/5/6) and a single catalytic enzyme at the base, DIS3. B) A structural model of human RNA exosome interacting with the essential helicase MTR4 is shown. The structure was generated using PyMOL based on PDB: 6D6R (Weick et al., 2018).

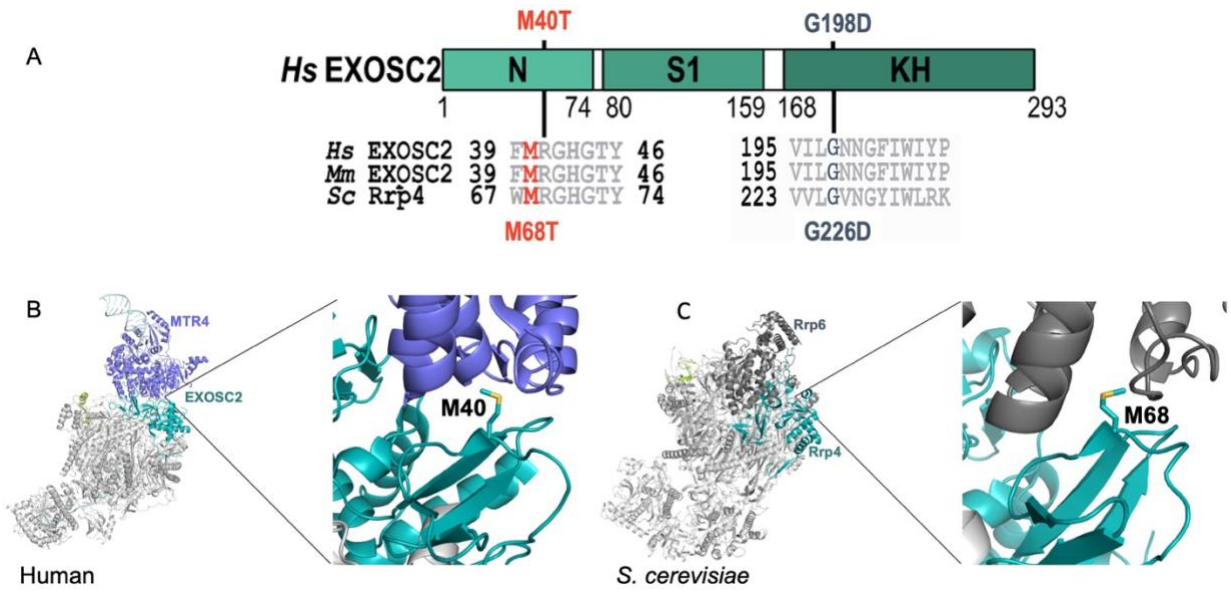

Figure 2. The EXOSC2 subunit of the RNA exosome is highly conserved. A) A domain schematic is shown of Hs EXOSC2 with the N-terminus, the S1 RNA binding domain, and the KH RNA binding domain of EXOSC2 indicated. The regions surrounding M40T and G198D in human EXOSC2, mouse EXOSC2, and *S. cerevisiae* Rrp4 with alignments are shown below. B) The location of EXOSC2 M40T in the nuclear human RNA exosome is on a key interface for interactions with cofactors including the essential RNA helicase MTR4 (PDB: 6D6R). The mutation was identified as a passenger mutation in a multiple myeloma patient. It is predicted to have an allelic frequency of 0.33 as the patient profile indicated trisomy of chromosome 9, as well as chromosomal translocation t(11;14), and a splice donor mutation; the patient is responding to initial therapy (NCT: MMRF2488). C) The location of Rrp4-M68T in the *S. cerevisiae* nuclear RNA exosome is on a key interface for interactions with cofactors including the 3'-5' exoribonuclease Rrp6 (PDB: 5VZJ).

A

Subunit	Rrp4		EXOSC2	
Mutation	M68T	G226D	M40T	G198D
Phyre²	Neutral	Damaging	Neutral	Damaging
PolyPhen-2 (HumDiv)	Probably Damaging (0.985)	Probably Damaging (1.000)	Possibly Damaging (0.543)	Probably Damaging (1.000)
PolyPhen-2 (HumVar)	Probably Damaging (0.963)	Probably Damaging (1.000)	Possibly Damaging (0.676)	Probably Damaging (0.999)
PROVEAN	Deleterious (-5.956)	Deleterious (-6.517)	Deleterious (-5.107)	Deleterious (-6.35)
SNAP2	Effect (61)	Effect (92)	Effect (53)	Effect (94)

B

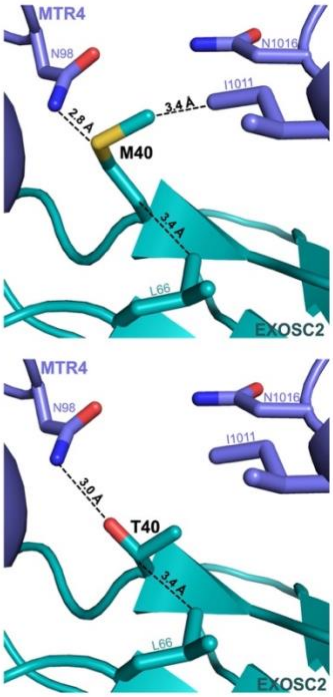

C

Subunit	Mutation	Hydrophobicity (WT/mutant)	Charge (WT/mutant)	Torsion	Predicted Affinity Change (kcal/mol) ($\Delta\Delta G^{Affinity}$)
EXOSC2 (human)	M40T	Hydrophobic/Neutral	No Charge	Favored	-0.55 (Decreasing)
	G198D	Neutral/Hydrophilic	No Charge/Charge	Favored	-0.509 (Decreasing)
Rrp4 (yeast)	M68T	Hydrophobic/Neutral	No Charge	Favored	-0.297 (Decreasing)
	G226D	Neutral/Hydrophilic	No Charge/Charge	Favored	-1.012 (Decreasing)

Figure 3. *In silico* predicted structural and biochemical effects of *Rrp4-M68T* missense mutation. A) I*n silico* predictions of the structural impact of EXOSC2-M40T and EXOSC2-G198D, Rrp4-M68T and Rrp4-G226D generated using Phyre², PolyPhen-2, PROVEAN, and SNAP2. B) EXOSC2 M40 and EXOSC2 T40 show different residue interaction distances with surrounding amino acids. EXOSC2 M40 is 2.8 A from MTR4 N98, 3.4 A from MTR4 I1011, 3.4 A from EXOSC2 L66, and 3.7A from MTR4 N1016. EXOSC2 T40 is 3.0 A from MTR4 N98, 4.5 A from MTR4 I1011, 3.4 A from EXOSC2 L66, and 4.7A from MTR4 N1016 (not all distances shown). C) *In silico* predictions of biochemical changes resulting from EXOSC2 M40T and G198D, Rrp4 M68T and G226D generated using Phyre² and mCSM-PPI2.

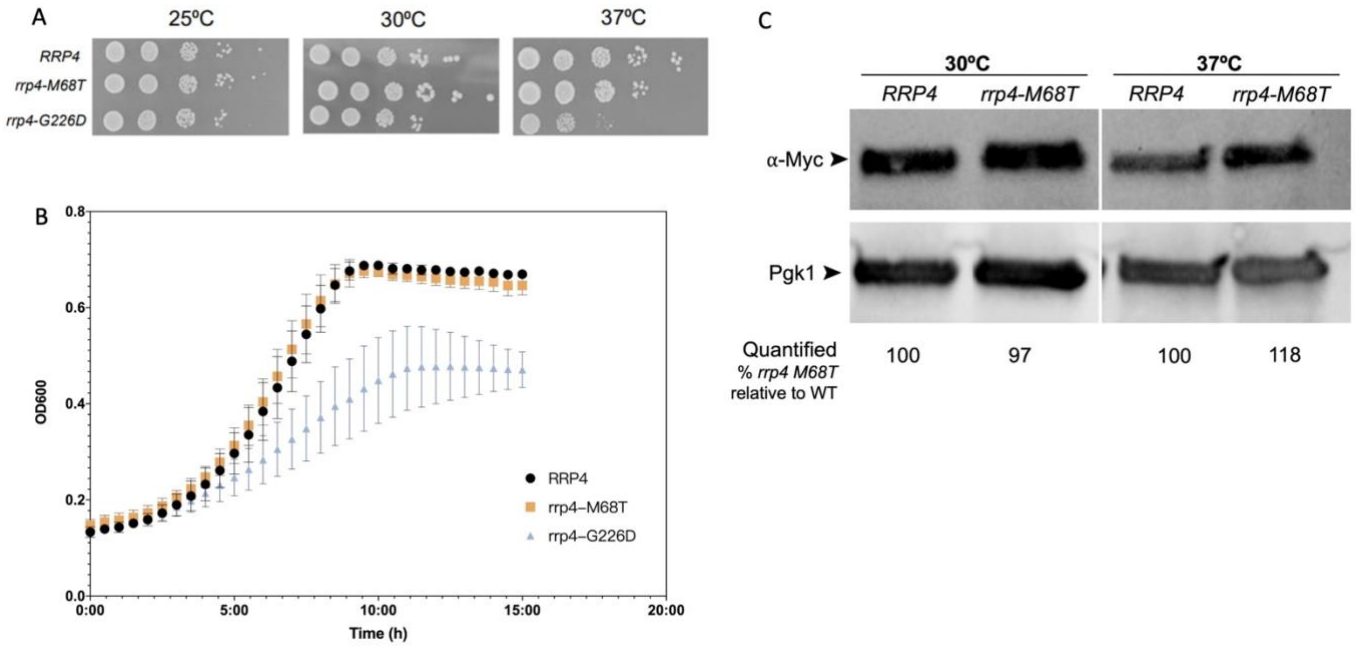

Figure 4. Serial dilution growth assay, growth curves and protein quantification in *S. cerevisiae* show no significant effects for rrp4-M68T. A) Serial dilution growth assay analyzing control *RRP4, rrp4-M68T*, and *rrp4-G226D* cells at 25°C, 30°C, 37°C. The *rrp4-G226D* cells show impaired growth at 37°C (n=8). B) Growth curves for control *RRP4, rrp4-M68T*, and *rrp4-G226D S. cerevisiae* cells at 37°C were generated by measuring optical density at a wavelength of 600nm. The *rrp4-G226D* cells show impaired growth. Three biological and three technical replicates were conducted for each sample. C) Immunoblot analysis of Myc-tagged RRP4 and Rrp4-M68T using Pgk1 as loading control is shown. Quantification was performed using ImageJ. Levels of Rrp4-Myc/Rrp4-M68T were normalized to Pgk1 loading control in each sample. The percentage of Rrp4-M68T-Myc was calculated relative to Rrp4-Myc at both temperatures (n=1).

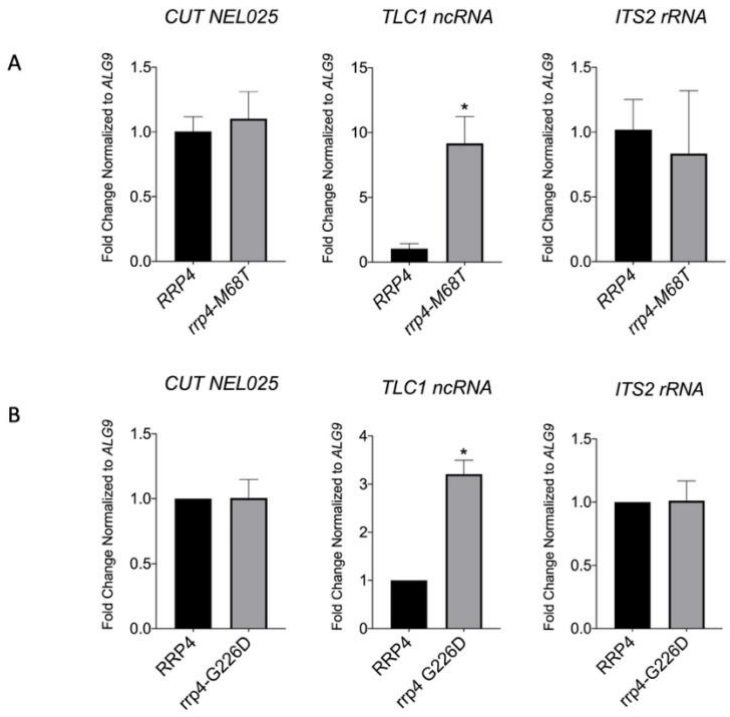

Figure 5. There are changes in steady state levels of the known RNA exosome target non-coding RNA *TLC1* in *rrp4-M68T* cells. A) Analysis using qPCR of known RNA exosome target RNAs: *CUT NEL025, TLC1 ncRNA,* and *ITS2 rRNA* in *RRP4* and *rrp4-M68T* cells. The analysis used a ΔΔCT approach relative to the loading control *ALG9* levels. The fold change of the target transcripts in *rrp4-M68T* cells was calculated relative to the same transcripts in control *RRP4* cells. B) A qPCR analysis of *CUT NEL025*, *TLC1* ncRNA, and *ITS2* rRNA was conducted in control *RRP4* and *rrp4-G226D* cells. Delta CT values were calculated relative to loading control *ALG9* levels. The fold change of the target transcripts in *rrp4-G226D* cells were calculated relative to transcript levels in control *RRP4* cells. Transcript levels in the control *RRP4* cells were set to 1.0. Data are presented as the means of triplicate biological replicates and the standard error of the mean (* symbolizes a p-value <0.05 in a two tailed t-test).

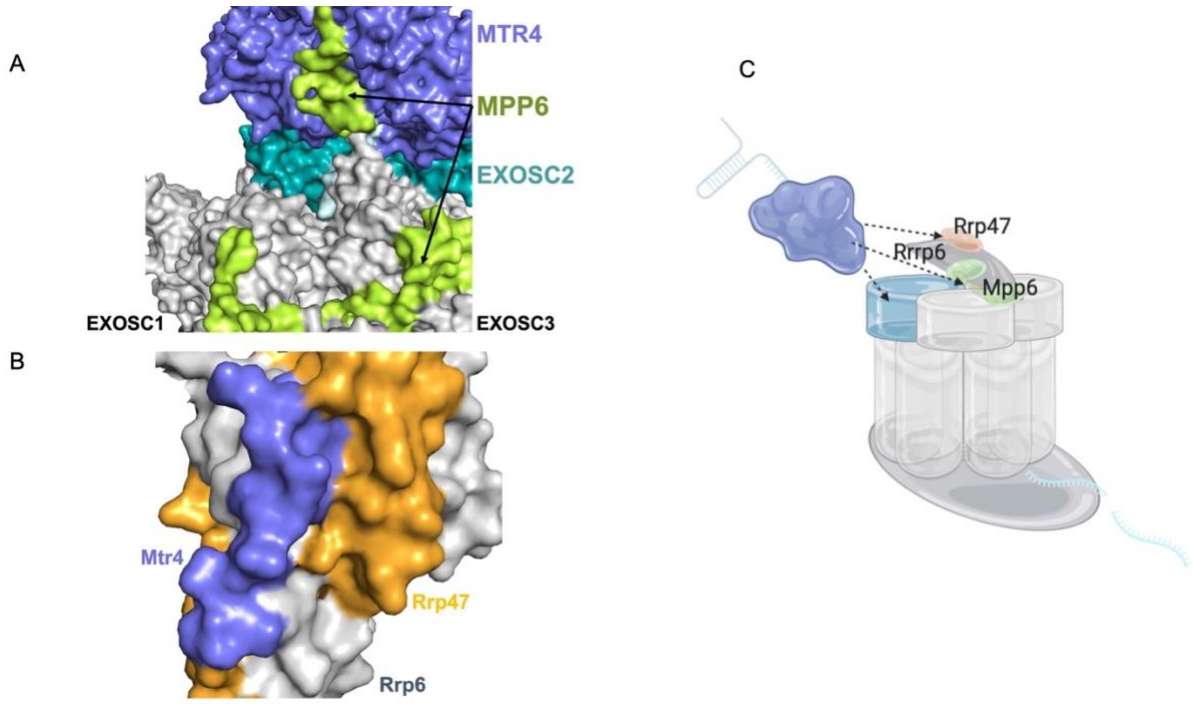

Figure 6. The cofactors RRP47 and MPP6 are important stabilizing partners for the interaction between the essential RNA helicase MTR4 and the RNA exosome. A) In the human nuclear RNA exosome, MPP6 serves as an anchor between MTR4 and the cap subunit of the RNA exosome, EXOSC3. The structure was generated using PyMOL from PDB: 6D6R; Weick et al.. B) In *S. cerevisiae*, Rrp47 coordinates important interactions of cofactors with the RNA exosome including the 3'-5' exoribonuclease Rrp6. The structure was generated using PyMOL from PDB: 4WFD (Schuch et al., 2014) C) An RNA exosome model identifying three stabilizing points for MTR4 to the RNA exosome, RRP47, MPP6, and EXOSC2/Rrp4 is shown.

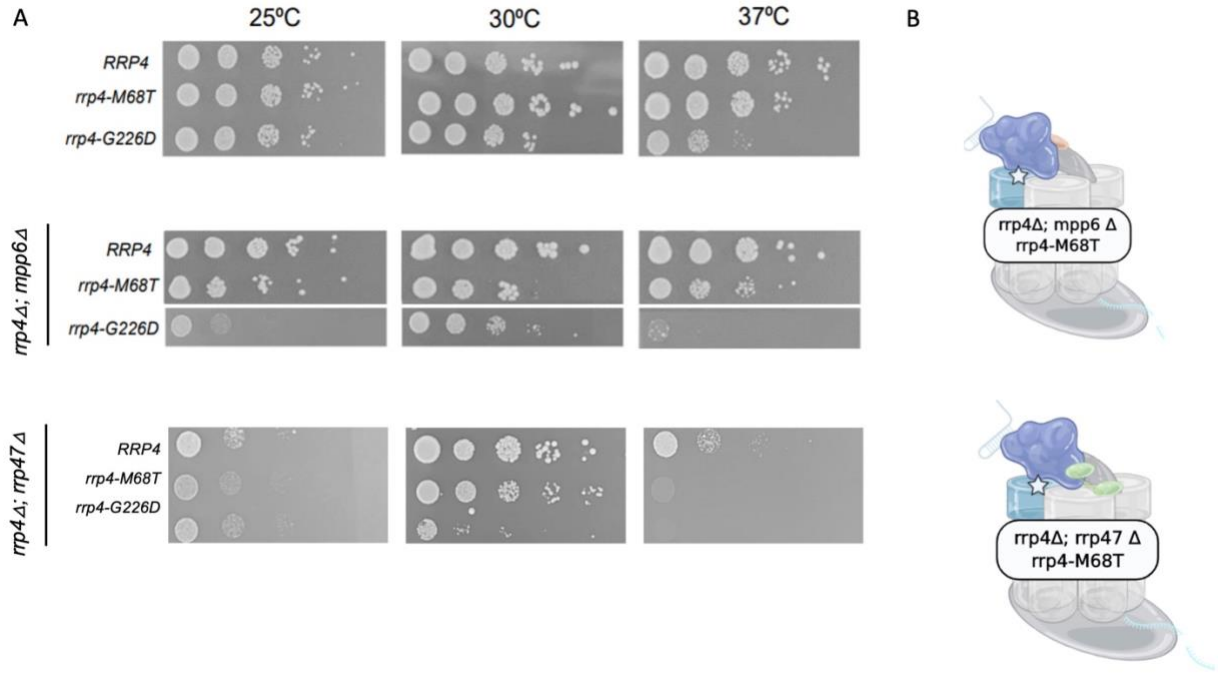

Figure 7. Deletion of *RRP47* or *MPP6* in *rrp4-M68T* cells causes impaired growth at 25°C and 37°C. A) Serial dilution growth assay of *Δmpp6 RRP4, Δmpp6 rrp4-M68T*, *Δmpp6 rrp4-G226D,* and *Δrrp47 RRP4, Δrrp47 rrp4-M68T*, *Δrrp47 rrp4-G226D* cells*. Δmpp6 rrp4-M68T* and *Δrrp47* rrp4-M68T show impaired growth at all temperatures analyzed. The growth defects observed for the *Δmpp6 rrp4-G226D* and *Δrrp47 rrp4-G226D* serve as controls (n=5) (Sterrett et al., 2020). B) RNA exosome models as visual representations to illustrate the mutants analyzed here *Δmpp6* and *Δrrp47*.

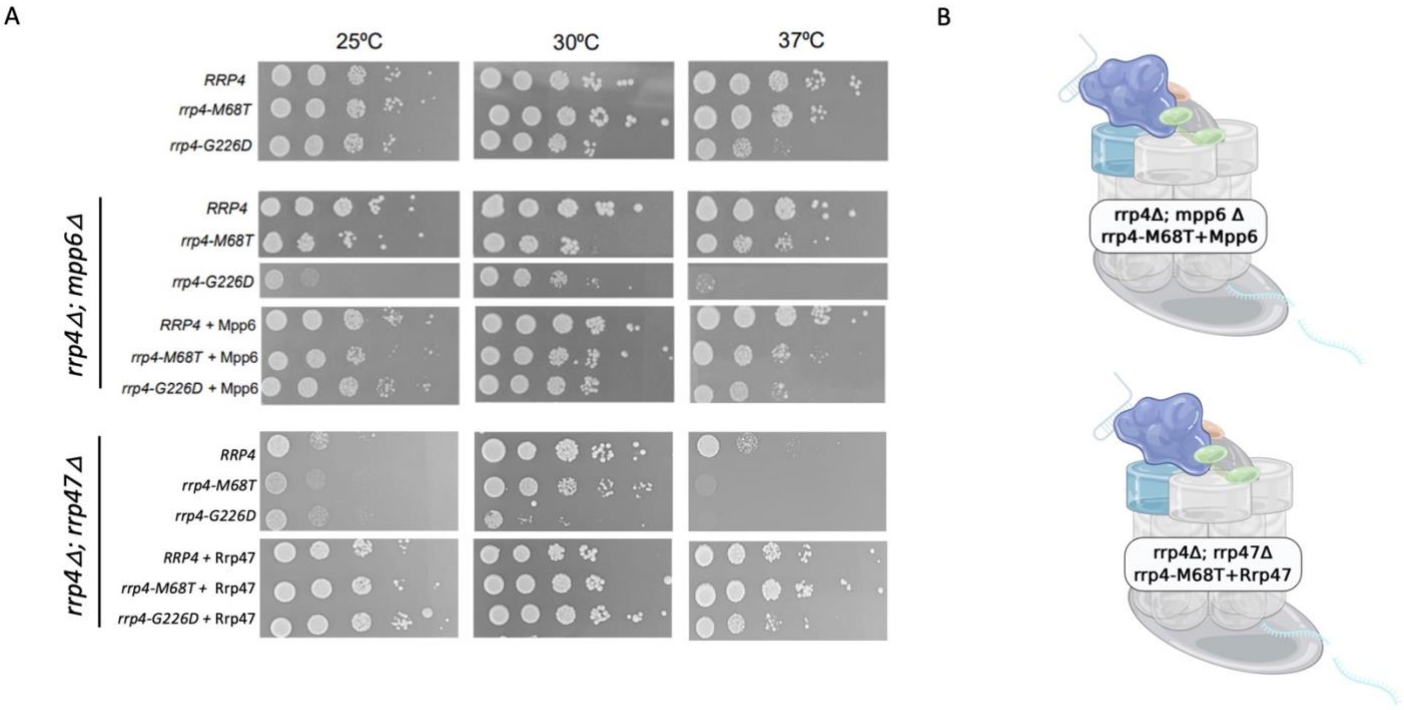

Figure 8. The growth phenotype of *rrp4-M68T mpp6Δ* and *rrp4-M68T rrp47Δ* cells can be rescued. A) Mpp6 or Rrp47 were expressed on plasmids in either *mpp6Δ* or *rrp47Δ* deletion mutants with *RRP4, rrp4-M68T*, or *rrp4-G226D* as indicated*. rrp4-M68T+Mpp6 mpp6Δ* and *rrp4-M68T+Rrp47 rrp47Δ* growth shows rescue at 25°C and 37°C relative to *rrp4-M68T mpp6Δ* or *rrp4-M68T Δrrp47* (n=5). B) RNA exosome models to illustrate the experiments for *rrp4-M68T+Mpp6 Δmpp6* and *rrp4-M68T+Rrp47Δrrp47* shown in A.

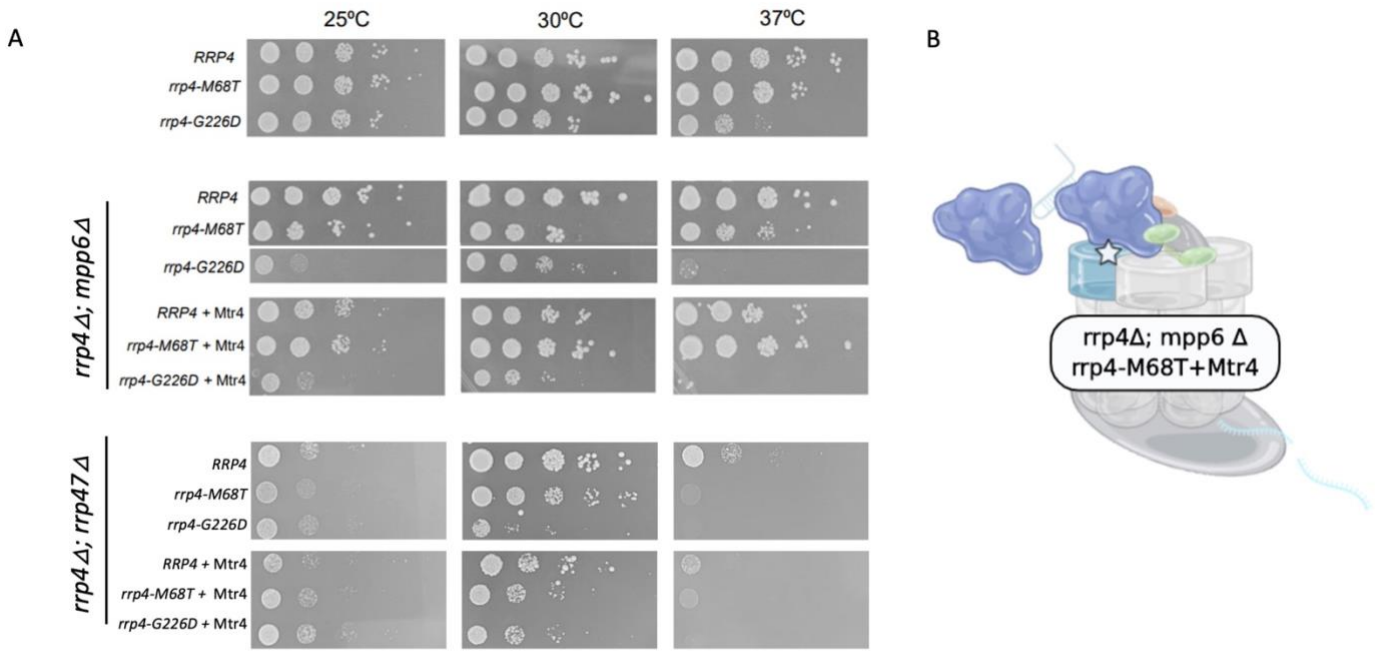

Figure 9. Mtr4 overexpression rescues in the growth defect of *rrp4-M68T mpp6Δ* cells. A) Mtr4 was expressed on a plasmid in the *mpp6Δ* or *rrp47Δ* deletion mutants with *RRP4, rrp4-M68T*, or *rrp4-G226D*s. The *rrp4-M68T+Mtr4 mpp6Δ* show rescued growth at 25°C and 37°C as compared to *rrp4-M68T mpp6Δ* alone. As controls, *RRP4+Mtr4 mpp6Δ*, and *rrp4-G226D+Mtr4 mpp6Δ* do not show rescued growth. Only a slight improvement in growth is observed for *rrp4-M68T Δrrp47* and *rrp4-G226D+Mtr4 Δrrp47* at 25°C (n=3). B) RNA exosome models illustrate the experimental set up for *rrp4-M68T+Mtr4 Δmpp6* in A.

SUPPLEMENTAL MATERIAL

Table 1. Yeast Strains and Plasmids used in this study.

Strain/Plasmid	Description	Source
rrp4Δ (yAV1104)	MATa his3Δ1 leu2Δ0 ura3Δ0 lys2Δ0 rrp4Δ::NEO [RRP4,URA3]	(Schaeffer et al., 2009)
rrp4Δ mpp6Δ	yAV1104 with *MPP6: NAT*	This study
rrp4Δ rrp47Δ	yAV1104 with *RRP47: NAT*	This study
pRS315	CEN6l LEU2, amp^R	(Sikorski and Hieter, 1989)
pRS426	URA3, 2-micron, amp^R	(Sikorski and Hieter, 1989)
pAC3474	RRP4-2xMyc in pRS315, CEN6, LEU2, amp^R	(Sterrett et al., 2020)
pAC3477	rrp4-G226D-2xMyc in pRS315, CEN6, LEU2, ampR	(Sterrett et al., 2020)
pAC2897	MTR4 in pRS426	This study
pAC3431	MPP6 in pRS426	This study
pAC3432	RRP47 in pRS426	This study

Table 2. DNA Oligonucleotides used in this study for quantitative RT-PCR.

Description	Sequence (5'-3')	Name
pre-U4 snRNA Fwd	AAAGAATGAATATCGGTAATG	AC5722
pre-U4 snRNA Rev	ATCCTTATGCACGGGAAATACG	AC5723
ITS2 rRNA Fwd	AGATTAGCCGCAGTTGG	AC7749
ITS2 rRNA Rev	AGCGTCATTTCCTTCTCA	AC7748
TLC1 ncRNA Fwd	AAGGCAAGGGTGTCCTTTCT	AC6420
TLC1 ncRNA Rev	TTCCGCTTGGAAAATAATGC	AC6421
ALG9 mRNA Fwd	CACGGATAGTGGCTTTGGTGAACAATTAC	AC5067
ALG9 mRNA Rev	TATGATTATCTGGCAGCAGGAAAGAACTTGGG	AC5068